International Journal of Concrete Structures and Materials
Vol.10, No.3, pp.325–335, September 2016
DOI 10.1007/s40069-016-0148-5
ISSN 1976-0485 / eISSN 2234-1315

Anchorage Effects of Various Steel Fibre Architectures for Concrete Reinforcement

Sadoon Abdallah, Mizi Fan*, Xiangming Zhou, and Simon Le Geyt

(Received January 11, 2016, Accepted May 2, 2016, Published online May 26, 2016)

Abstract: This paper studies the effects of steel fibre geometry and architecture on the cracking behaviour of steel fibre reinforced concrete (SFRC), with the reinforcements being four types, namely 5DH (Dramix® hooked-end), 4DH, 3DH-60 and 3DH-35, of various hooked-end steel fibres at the fibre dosage of 40 and 80 kg/m^3. The test results show that the addition of steel fibres have little effect on the workability and compressive strength of SFRC, but the ultimate tensile loads, post-cracking behaviour, residual strength and the fracture energy of SFRC are closely related to the shapes of fibres which all increased with increasing fibre content. Results also revealed that the residual tensile strength is significantly influenced by the anchorage strength rather than the number of the fibres counted on the fracture surface. The 5DH steel fibre reinforced concretes have behaved in a manner of multiple crackings and more ductile compared to 3DH and 4DH ones, and the end-hooks of 4DH and 5DH fibres partially deformed in steel fibre reinforced self-compacting concrete (SFR–SCC). In practice, 5DH fibres should be used for reinforcing high or ultra-high performance matrixes to fully utilize their high mechanical anchorage.

Keywords: steel fibre, post-cracking behaviour, self-compacting concrete, fibre orientation, fracture energy and residual strength.

1. Introduction

It is well known that an addition of fibres to concrete is able to improve their tensile strength, fracture energy absorption and load bearing capacity (Romualdi et al. 1968; Naaman 1972; Swamy 1975; Banthia and Trottier 1991; Abrishambaf et al. 2013; Zhang et al. 2014; El-Mal et al. 2015; Li and Liu 2016). The fibre contribution is mainly reflected when the concrete cracking initiates and often enhances the post-cracking behaviour due to the improved stress transfer provided by the fibre bridging of the cracked sections (Islam and Alam 2013; Tadepalli et al. 2015; Srikar et al. 2016). The most important parameter of fibres is their ability to transfer stresses across cracked sections rather uniformly (Pająk and Ponikiewski 2013; Sorensen et al. 2014).

The mechanical properties and post-cracking behaviour of steel fibre reinforced concrete (SFRC) greatly depend on the matrix properties in addition to the concentration, type, geometry, orientation and distribution of fibres, while the efficiency of fibre reinforcement depends on the deformed shape of the fibres, which enhances the anchorage mechanisms during the pulling-out.

While various fibres can be used for concrete reinforcement, approximately 67 % of commercial fibres are the hooked-end fibres, around 9 % for both straight and deformed wire, 9 % for crimped fibres and 15 % for other steel fibre types (Pająk and Ponikiewski 2013). The variety of reinforcing fibres may have a significant effect on the efficiency of the reinforcement, hence, research on the design and architecture of fibres has been an interesting area for the researchers and engineers in the sector. For example, Bekaert has recently redesigned and expanded its Dramix® range of hooked-end steel fibres, and introduced the new generation of 4DH and 5DH series of Dramix®, the unique shape and performance of which could open up a new level of possibilities for design and construction.

The distribution and orientation of fibres in hardened concrete are very much dependant on its fresh-state characteristics after mixing, namely, flowability, casting method, vibration and wall-effects introduced by the formwork (Abrishambaf et al. 2013; Laranjeira de Oliveira 2010). Tremendous scatterings in the bending test results of SFRC have been reported in the literature (Şanal and Özyurt Zihnioğlu 2013). The main reason for this phenomenon is because of high variation in fibre distribution and orientation (Ferrara et al. 2012; Kooiman 2000; Vandewalle 2000). It has been observed that an alignment of fibres in the direction of flow resulted in better post-cracking properties compared to those in the perpendicular direction (Abrishambaf et al. 2013).

To overcome the aforementioned deficiencies, the combination of steel fibres and self-compacting concrete (SCC) has quickly become one of the common concrete technologies in the construction industries (Ferrara et al. 2012). Several studies have demonstrated that the main benefits of

Department of Civil Engineering, Brunel University London, London UB8 3PH, UK.
*Corresponding Author; E-mail: mizi.fan@brunel.ac.uk

adding steel fibres in self-compacting concrete are to achieve uniform distribution of fibres in the matrix as well as rheological stability without compaction and vibration (Ozyurt et al. 2007; Ferrara and Meda 2006). This indicates that fibre dispersion and orientation could be crucial for the key properties of steel fibre reinforced self-compacting concrete (SFR–SCC), and the link between its fresh- and hardened-state performances (Ferrara et al. 2012). Numerous methods have been adopted in literature to evaluate performance of steel fibre reinforced concrete (SFRC), with the uniaxial tensile and flexural tests being the most commonly ones (Rilem; Wecharatana and Shah 1983; Gopalaratnam and Gettu 1995; Kooiman 2000; Ding 2011).

Many national and international technical committees have also proposed recommendations and guidelines to analyse the post-crack behaviour of SFRC based on the load–deflection diagrams and the load–CMOD diagrams, for example, RILEM TC162-TDF recommendation (Vandewalle 2000) and those very similar to it such as EN 14651(EN 2007), ASTM C1018 (Astm, 1994), CNR-DT 204(CNR, 2006) and JSCE method (JSCE-SF4 III, 1984). Nevertheless, there is little information of repeatable database for understanding the correlation of variety of fibre types with concrete behaviour, particularly for these new types of fibres.

The main objectives of this study are to examine and compare post-cracking tensile behaviour of self-compacting concrete reinforced with four different types of hooked-end steel fibres, and to investigate the influence of new shape hooked-end steel fibres (4DH and 5DH) on post-peak behaviour of the reinforced concrete. The orientation and distribution of steel fibres on the fracture section have also in particular been considered for analysing the influence of flowablitity properties on the performance of hardened SFRC. The quantitative analyses are performed to compare the behaviour of old generation steel fibres (3DH) and new ones (4DH and 5DH) to assess the development and the positive effect of the newly developed shapes of steel fibres.

2. Materials and Methods

2.1 Materials and Mix Design

The following constituent materials were used for the formulation of the SFR–SCC: Portland-limestone cement CEM II 32,5R, fly ash EN-450, combination of two particle sizes of crushed granite aggregates which consisted of 60 % of (6 mm) and 40 % of (10 mm), sand, superplasticizer TamCem (23SSR) and water. For all mixes, the proportion of the ingredients maintained the same and only the fibre content varied as presented in Table 1. Four types of Dramix® hooked-end steel fibres were selected, each of them added at two levels of dosage of 40 and 80 kg/m^3, corresponding approximately to a volume fraction of 0.5 and 1 % respectively. All these types of fibres have the same length 60 mm and aspect ratios ($l/d = 65$), except (3DH-35), which is 35 mm. The properties of the steel fibres are presented in Table 2. During concrete casting, the raw materials (cement, fly ash, crushed granite and sand) were firstly dry mixed for 1 min for homogeneity and then 80 % of water and superplasticizer were added to the dry mixture which was then mixed for 4 min. Finally, since the hooked-end fibres are glued into strips, the remaining water and fibres were added simultaneously to dissolve the glue and distribute the fibres in the mixer and the whole mixture was further mixed for 3 min.

2.2 Sample Preparation

Twenty seven beams all with the dimensions of 150 × 150 × 600 mm^3 were cast for SCC and SFR–SCC mixtures. All beams were cast by using the flowed mix from one end of the mould to the other end until the mould was full. All the test specimens were removed from the moulds after 24 h and cured for further 27 days in a chamber (20 ± 2 °C, 96 ± 5 % RH). All series were coded: the first number and letter denotes the fibre type (3DH, 4DH and 5DH), the second number the fibre length in mm and the last group number the fibre content in kg.

2.3 Experiment

Three-point bending tests on notched beams having dimensions 150 × 150 × 600 mm^3 were performed in accordance with RILEM TC 162-TDF(RILEM 2001). In the mid-span of each beam, a single notch with depth of 25 mm and width of 3 mm was cut to localize the crack. The beams were placed on roller supports, so to have a test span of 500 mm (see Fig. 1a). It should be noted that each beam is turned 90° from the casting surface, and the notch is then sawn through the width of the beam at mid-span. The tests were carried out by imposing a constant displacement rate of 0.5 mm/min under the INSTRON 5584 electromechanical testing machine. The test was controlled by means of crack mouth opening displacement (CMOD), using a clip-on extensometer with a ±2.5 mm range and 10 mm gauge length. The mid-span deflection was also measured using a yoke mounted on the tested beams (see Fig. 1b).

Table 1 Mixture proportion per 1 m^3 of concrete made.

Cement CEM II/A-L 32,5R (kg/m^3)	Fly ash (kg/m^3)	Sand (0–2 mm) (kg/m^3)	Coarse aggregate (6–10)mm (kg/m^3)	Steel fibres (kg/m^3) (%)	Superplasticizer (l/m^3)	Water (l/m^3)	W/C
C	FA	S	CA	SF	SP	W	–
470	45	850	886	40;80(0.5;1)	6	216	0.42

Table 2 Properties of steel fibres.

Fibre type	Diameter (mm)	Length (mm)	Aspect ratio –	No. fibre per kg	Tensile strength (MPa)	Young's modulus (MPa)
3D 65/35 BG	0.55	35	65	14,531	1345	±210,000
3D 65/60 BG	0.90	60	65	3183	1160	±210,000
4D 65/60 BG	0.90	60	65	3183	1500	±210,000
5D 65/60 BG	0.90	60	65	3183	2300	±210,000

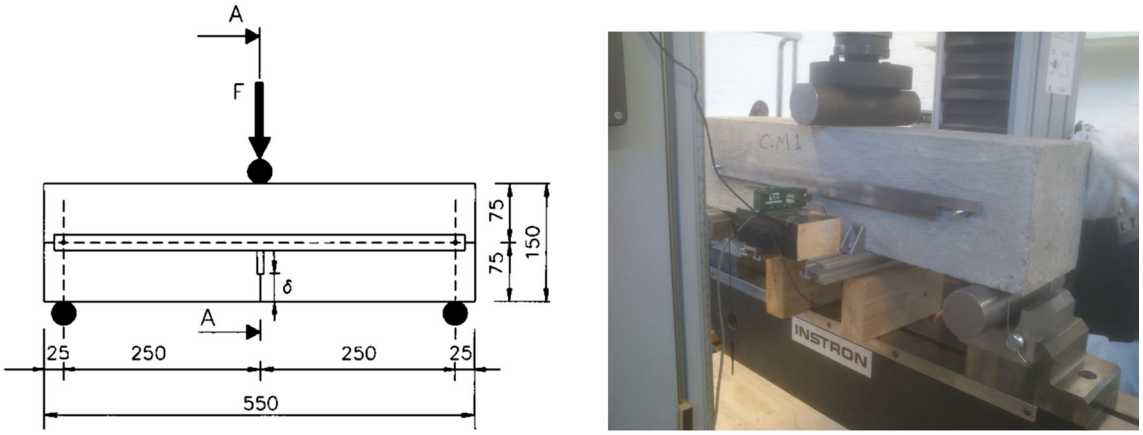

(a) Specimen dimensions **(b)** Test setup

Fig. 1 Arrangement of three-point bending test **a** specimen dimensions and **b** test setup.

3. Results and Discussions

3.1 Effect of Steel Fibres on Rheology of Paste and Compressive Strength of Hardened SFR–SCC

To evaluate the rheological and self-compactable properties of fresh SFRC, the slump-flow test was performed according to EN 12350-8: 2010 (EN, 2007). It appears that all mixtures had stable and excellent self-compacting properties (Table 3), although adding steel fibres slightly affect the workability of SFRC-SCC. The slump-flow diameter (SFD) and time to reach 500 mm spread (T50) of the fresh concrete are also very similar between the mixtures. The inclusion of steel fibres has not affected the density of SFRCs, although it slightly increases their compressive strength. In addition, since 3DH-60, 4DH and 5DH have the same length and aspect ratio, the different shape of the hooked-end is not a sufficient factor to induce a significant variation in slump flow diameter as it does on compressive strength as expected.

3.2 Effect of Various Hook Ends of Steel Fibre on the Peak and Residual Loads of SFR–SCC

A comparison of typical load-CMOD curves of plain SCC beams and SFC–SCC beams reinforced by different hooked-end steel fibres at various dosages are presented in Figs. 2

Table 3 Properties of fresh and hardened SFR–SCC mix.

Mix	Slump flow test		Density (kg/m^3)	$f^{a}_{cm,28d}$(MPa)	CV (%)
	$T_{500\ (S)}$	SFD (mm)			
CM	2	710	2398	49.86	5.32
3D-30-40	1	700	2295	47.45	4.40
3D-30-80	1	700	2349	46.79	4.44
3D-60-40	2	700	2348	48.52	5.18
3D-60-80	2	695	2372	48.24	5.50
4D-60-40	2	700	2366	49.75	7.06
4D-60-80	1	695	2321	48.67	6.28
5D-60-40	1	700	2375	49.85	3.07
5D-60-80	1	700	2385	50.5	4.88

[a] Average of three specimens.

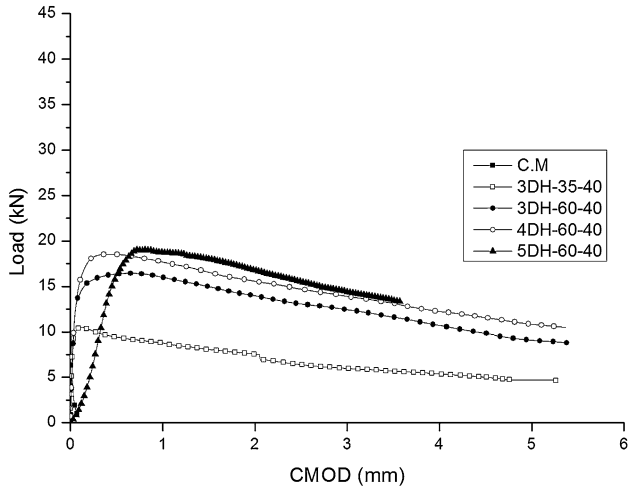

Fig. 2 Comparison of load-CMOD curve of SFR–SCC series reinforced with 40 kg fibres.

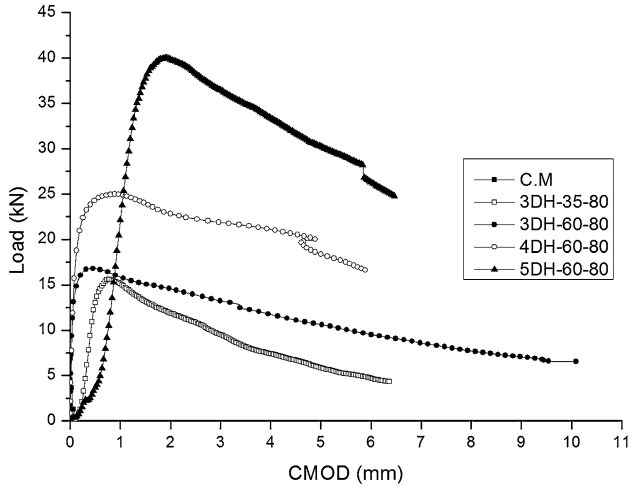

Fig. 3 Comparison of load-CMOD curve of SFR–SCC series reinforced with 80 kg fibres.

and 3. It can be seen that all plain concrete beams exhibit almost linear-elastic behaviour up to the peak load, followed by a sudden drop in load, upon which the beams separated into two parts. On the other hand, the beams reinforced with steel fibres demonstrated not only significantly higher peak load, but also a tri-linear load-CMOD behaviour with a multiple cracking process before localizing into a single major crack. Continuing crack propagation existed after peak load due to the crack control effect of fibres on the cracked surface. Once the micro-cracking propagates and joins together into larger macro-cracks, the series reinforced with long hooked-end fibres (i.e. 60 mm) became more effective in crack bridging than those series with short hooked-end fibres (i.e. 35 mm) (see Figs. 2 and 3). This mainly due to the high anchorage strength provided by the hook especially of 4DH and 5DH fibres which results in a high resistance to cracks propagation. For the concrete reinforced by 60 mm fibres at the dosage of 40 kg/m^3, the peak loads are about 15, 13 and 18 kN for those with the 3DH-60, 4DH and 5DH fibres, and for the concrete reinforced by 60 mm fibres at the dosage of 80 kg, these values increased to 18, 26 and 40 kN, compared to 8 kN for the plain concrete one. For the beams reinforced by 3DH fibres, the peak loads are 12 and 15 kN in case of 35 and 60 mm long fibres, respectively, at the dosage of 40 kg fibres and these values increased to 16 and 18 kN, respectively at the dosage of 80 kg.

After peak load was reached, the load carrying capacity deterioration started, the lower the fibres content, the higher the loss of strength. The load bearing capacity descends immediately after the first visible crack initiated, which may be attributed to the bond slip of some fibres at the cracked surface. This also reflected the higher loss of strength for the shorter fibre reinforced concrete as the short fibre may be relatively easier to be pulled out. Gradual reduction of loading capacity continues until all fibres slip from the cracking regions. As mentioned, the maximum load increases with an increase of fibre content for all four types of hooked-end steel fibres. However, the residual load of the tested beams with long fibres also shows a more ductile trend than that with short fibres over the entire CMOD range. This may be attributed to the positive effect of long steel fibres, as the short fibres are gradually pulled out with the increase of the CMOD, while the high mechanical anchoring provided by the lengthy hook of 4DH and 5DH fibres continues to transfer the stress between fibres and matrix, generating higher strain and stress (residual load) at the post-cracking stage.

A comparison among various hooked-end types of fibre, for the same fibre content, showed that the order of performance in terms of peak load is 5DH->4DH->3DH-60->3DH-30. The beams reinforced with series of 5DH-60-80 feature higher ultimate load than the other hooked-end ones (Fig. 3). For the long hooked-end fibres reinforced concrete with the same fibre content, even though they have somewhat equal number of fibres on fracture surface, different peak loads existed among them, showing that the peak loads of SFR–SCC is strongly affected by the hook shape of fibres.

The residual load of the beams evaluated at 4 mm CMOD is about 91, 87, 79 and 53 % of their peak load for the series reinforced with 80 kg/m^3 of 5DH, 4DH, 3DH-60 and 3DH-30 respectively. The high residual load obtained from the series reinforced with 5DH may be the result of a unique combination of a lengthy hook, a high ductility wire and high tensile strength. Regarding the series reinforced with 5DH fibres, there is also a noteworthy observation; the CMOD value corresponds to the maximum load is equal to 2 mm, while relatively small CMOD values (less than 0.7 mm) were registered for the other types of the hook ended fibres. In the case of the series reinforced with 3DH-35, the decrease of the residual load up to 53 % of its peak load was observed, mainly due to the fibre pulled out and fully deformed at small crack widths. On the other hand, the series reinforced with 5DH fibres showed high resistance to fibre pullout and resulted in somewhat lower regression of residual peak load at larger crack widths. Thus it could be attributed to the fact that the fibre mechanical anchorage is much higher for 5DH fibres than those offered by other hooked-end fibre types.

3.3 Effect of Various Hook Ends of Steel Fibre on the Post Cracking Tensile Behaviour

To evaluate the post-cracking tensile behaviour of SFRC, 3-point bending test according to RILEM TC 162-TDF was performed (RILEM 2001). The main benefits of using RILEM TC162-TDF recommendation is to obtain dimensional parameters representative of the post-peak behaviour to be used in SFRC structural design (Giaccio et al. 2008). From this method, two possible groups of material parameters can be obtained to characterize the post cracking behaviour: the first group is the residual flexural tensile strengths and the second one is equivalent flexural tensile strengths. The first crack load or the load at the limit of proportionality, F_L, can be determined as the highest value of the load in the interval (δ or CMOD) of 0.05 mm. The strength corresponding to the limit of proportionality (LOP) can be obtained by using the following equation:

$$f_{\mathrm{fct,L}} = \frac{3.F_L.l}{2.b.h_{sp}^2}(\mathrm{Mpa}) \quad (1)$$

where, l (500 mm), b (150 mm) and h_{sp} (125 mm) are the span of the specimen, width and distance between the tip of the notch and the top of the specimen, respectively.

To assess the post-peak behaviour of SFRC, the residual flexural tensile strengths, $f_{R,1}$, $f_{R,2}$, $f_{R,3}$ and $f_{R,4}$, corresponding to the values of $\mathrm{CMOD}_1 = 0.5$ mm, $\mathrm{CMOD}_2 = 1.5$ mm, $\mathrm{CMOD}_3 = 2.5$ mm and $\mathrm{CMOD}_4 = 3.5$ mm were also computed. The residual flexural strength is calculated according to the following expression:

$$f_{R,j} = \frac{3.F_{R,j}l}{2.b.h_{sp}^2}(MPa) \quad (2)$$

The mean value and the standard deviation of the post-peak parameters of all series from load-CMOD curves are given in Table 4. It is evident that overall the increase of fibre content significantly enhanced the residual strength of SFRC, except 3DH-35 SFRC. However, this may not solely be attributed to fibre content, since, for the series reinforced with 80 kg/m^3 hooked-end steel fibre, different post cracking behaviour was observed. It can be observed that the deformed shape of hooked-end fibre has a considerable effect on post-peak behaviour, especially, for series reinforced with 5DH hooked-end steel fibre. Since the aspect ratio and fibre content of all hooked-end fibre types were constant, the 5DH hooked end steel fibre is more effective in improving the post-peak parameters than the other hooked-end ones for both 40 and 80 kg/m^3 fibre dosage. It can also be observed that with an increase of the fibre dosage from 40 to 80 kg/m^3, the changes in the post-peak parameters appear to be more significant for the series with 5DH hooked-end steel fibre than for any other fibre types. This may be attributed to the bond strength between steel fibres and matrix with 5DH fibres featuring a desirable combination of hook shape, high ductility, and high tensile strength. It was also observed that for series with 3DH fibre, the majority of fibres were pulled out and the hooked-ends were straightened during the cracking process, while the fibres were not fully straightened in case of 4DH and 5DH fibres (see Fig. 4). Therefore, the fibres with higher deformed shape and tensile strength would be more effective if these types of fibres are used in high or ultra-high performance concrete to obtain high mechanical bond between fibre and matrix. It must also be observed that, as generally known in the literature, fibres with high aspect ratio can significantly enhance post cracking parameters of SFRC. In this study, however, fibres with equal aspect ratio (i.e. l/d = 65) but different length were used, and the results have revealed that the post cracking behaviour is also largely influenced by the shape and length of fibres.

3.4 Fracture Energy

To evaluate the fracture energy of SFRC, the results of area under the load-CMOD curve of a notched beam tested under three-point bending load were adopted according to RILEM TC 50-FMC (Rilem 1985). The fracture energy can be defined as the amount of the absorbed energy to form one unit area of a crack (Beygi et al. 2013; Pająk and Ponikiewski 2013). By dividing the total dissipated energy with

Table 4 Experimental results of post cracking parameters of SFR–SC.

Mix	F_L (kN)	Residual strength parameters (MPa)*				
		$f_{\mathrm{fct,L}}$	$f_{R,1}$	$f_{R,2}$	$f_{R,3}$	$f_{R,4}$
3D-35-40	11.30 (9.55)	3.61 (9.41)	3.39 (11.80)	2.80 (7.85)	2.17 (5.53)	1.90 (5.26)
3D-35-80	11.12 (16.54)	3.56 (16.29)	5.14 (5.05)	4.64 (4.95)	4.23 (5.67)	3.80 (5.26)
3D-60-40	13.43 (7.07)	4.29 (6.99)	5.62 (5.87)	5.21 (7.10)	4.56 (7.45)	4.05 (7.16)
3D-60-80	14.52 (8.05)	4.59 (4.35)	5.78 (5.19)	5.23 (7.26)	5.05 (8.91)	4.40 (6.13)
4D-60-40	8.51 (11.86)	2.72 (11.76)	4.86 (6.79)	4.31 (10.44)	3.64 (9.61)	3.09 (6.47)
4D-60-80	15.25 (10.29)	4.88 (10.24)	7.95 (2.01)	7.57 (2.90)	7.10 (1.97)	6.81 (3.37)
5D-60-40	0.97 (8.24)	0.31 (6.45)	4.94 (21.65)	5.51 (6.89)	4.51 (11.75)	3.80 (16.31)
5D-60-80	0.41 (53.65)	0.13 (53.84)	2.23 (51.12)	11.44 (4.89)	11.85 (2.86)	10.51 (5.70)

* Values in () = CV (%).

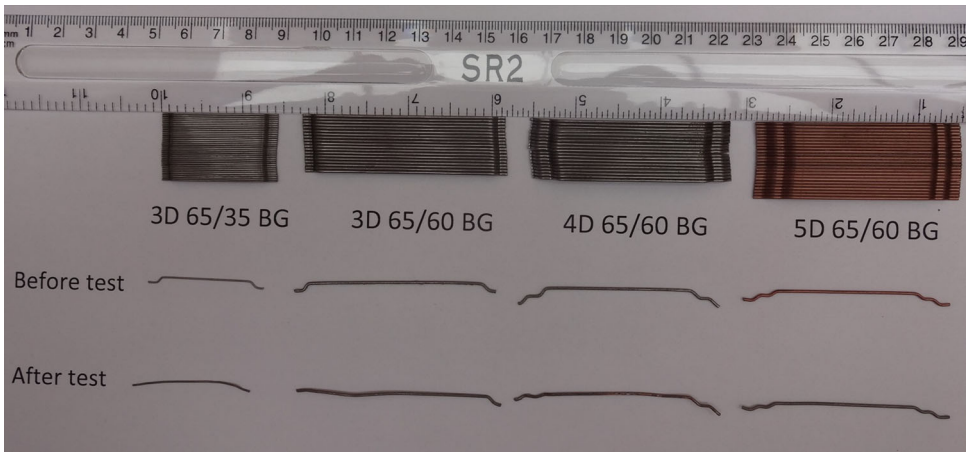

Fig. 4 Comparison of different hooked end steel fibres before and after fibre deformation.

the initial ligament area, the fracture energy is obtained as following expression:

$$G_F = \frac{W_o}{b(h - a_o)} \tag{3}$$

where, W_0 is the area under the load-CMOD curve, and b, h and a_0 represent the width, height and notch depth of beam respectively.

It has been recommended by Bencardino et al. (2013) that only the fracture energy absorbed up to a displacement of 3 mm is of interest from design point of view. Therefore in the present study, the fracture energy is calculated up to a CMOD value of 3 mm. It should be noted that a work of fracture has been computed and specify that no additional measure to clean the elastic energy effect has been taken.

Table 5 summarizes the results of the mean and coefficient variation of fracture energy obtained in this study. It can be observed that the fracture energy increases with increasing fibre content for all series, however, the fracture energy of series 5DH at 80 kg/m^3 dosage is significantly higher than that of other series with same fibre content. As expected, the new shape of 5DH steel fibres may offer higher levels of anchorage, tensile strength and ductility, which result in guaranteeing better performance. It can also be seen that the latter series showed a more ductile behaviour under flexural load with multiple cracking around the tip of the notch and this did not occur with other series. This fact can also be related to the fibre mechanical anchorage and such high fracture energy is required to create a crack. Since fracture energy significantly increased with increment of fibre content, the overall toughness can significantly be influenced by the shape of fibres.

3.5 Fibre Distribution and Effective Fibres

In order to assess the alignment and distribution of the steel fibres on the specimen's fracture surface, the total number of fibres visible on it and the number of fibres pulled out on the corresponding opposite sides were counted. To count the number of fibres on both fracture surfaces, the cross section of beam was divided into four rows and five columns. The fibres in each row, on both faces of the fractured beam were calculated. The total number of fibre per unit cross-sectional area of concrete can be computed by the following expression (Laranjeira de Oliveira 2010; Soroushian and Lee 1990):

$$N_f = \frac{A_{\text{sec}}}{A_{fib}} \times Vf \times a \tag{4}$$

where A_{sec} is the cross-sectional area of specimen (mm^2), A_{fib} is the cross-sectional area of steel fibres (mm^2), V_f is the volume fraction of fibres (%) and α is the orientation factor.

Table 5 Experimental results of fracture energy of SRF–SCC.

Mix	Mean G_F (N/m)	CV (%)
3D-30-40	1.13	9.02
3D-30-80	3.05	2.97
3D-60-40	1.94	11.78
3D-60-80	2.50	16.45
4D-60-40	1.34	18.34
4D-60-80	4.20	2.38
5D-60-40	2.14	11.71
5D-60-80	5.53	9.65

Table 6 Number of fibres counted on different locations of fractured cross sections.

Mix	Distance from the top (mm)	No. of fibres		% of fibres	Density	Orientation factor α	
		Mean	Cv (%)		Fibres/cm^2	Mean	SD
3D-35-40	Raw1	44	11.36	24.22	0.93	0.445	
	Raw2	46	8.69	24.95	0.96	0.459	0.01
	Raw3	48	10.41	26.42	1.02	0.486	
	Raw4	45	15.55	24.40	0.94	0.449	
3D-35-80	Raw1	85	12.94	22.63	1.80	0.428	
	Raw2	104	4.80	27.8	2.21	0.526	0.04
	Raw3	98	3.06	26.11	2.08	0.494	
	Raw4	88	5.68	23.44	1.87	0.444	
3D-60-40	Raw1	25	16	23.24	0.54	0.687	
	Raw2	29	6.89	26.29	0.61	0.777	0.03
	Raw3	28	21.42	25.68	0.59	0.759	
	Raw4	27	14.81	24.77	0.57	0.732	
3D-60-80	Raw1	48	16.66	25.66	1.02	0.651	
	Raw2	47	8.51	25.55	1.01	0.649	0.20
	Raw3	44	11.36	23.88	0.95	0.606	
	Raw4	46	15.21	24.77	0.98	0.628	
4D-60-40	Raw1	21	17.34	22.10	0.95	0.606	
	Raw2	23	10.26	24.21	0.98	0.628	0.01
	Raw3	28	13.85	29.47	1.01	0.642	
	Raw4	23	22.24	24.21	0.95	0.606	
4D-60-80	Raw1	47	19.14	26.60	0.99	0.664	
	Raw2	42	4.76	24.00	0.89	0.719	0.045
	Raw3	45	26.67	25.90	0.96	0.643	
	Raw4	41	17.07	23.42	0.87	0.611	
5D-60-40	Raw1	24	16.67	24.31	0.51	0.642	
	Raw2	26	26.92	26.71	0.55	0.705	0.03
	Raw3	24	20.83	24.65	0.52	0.651	
	Raw4	23	26.08	24.31	0.50	0.642	
5D-60-80	Raw1	46	15.21	25.37	0.97	0.619	
	Raw2	44	20.45	24.62	0.94	0.601	0.008
	Raw3	46	8.69	25.18	0.96	0.615	
	Raw4	45	17.77	24.81	0.95	0.610	

Table 6 summarizes the mean and variation of coefficient of number of fibres counted on different location of fractured cross section in of the 27 specimens. It can be seen that the number of fibres counted on fractured surface increases with increasing fibre content. Generally, very good distribution and orientation have been observed for all SFR–SCC series. This fact can be related to the casting method (flow method), which is able to produce a good alignment of fibres to the main tensile stress, regardless of the size and the shape of the specimen. However, from Table 6 no clear relation between the numbers of fibres counted on the fracture surface and residual tensile strength behaviour of SFRC can be found. Three reasons may explain this finding: (1) Although the beams reinforced with 3DH-35 fibres have the highest number of fibres that counted on fracture surface, a lower residual tensile strength is observed; (2) it is also evident

from Table 6 that these fibres also have lower values of orientation factor, indicating that less alignment of the fibres in the direction of flow leads to lower post-cracking strength; and (3) the residual tensile strength seems to be more influenced by the mechanical anchorage strength than the number of fibres that exists on the fracture surface.

On the other hand, the number of effective fibres on both fracture surfaces has been computed for each specimen, i.e. the fibres, whose hooked-ends were straightened during cracking bridging, were recorded. It must be noted that for the specimens reinforced with fibres 4DH and 5DH, the hook of most fibres did not deform in the cracking process (see Fig. 4). Therefore, the number of fibres with the hooks partially straightened has been recorded. It is clear that the number of effective fibres of the 3DH fibre reinforced concrete is higher than those of 4DH and 5DH ones. Nevertheless, it is evident that the residual strengths of SFRC are considerably affected by shape and length of hooked-end fibre than the number of fibres within the fracture zone.

It is interesting to note from Fig. 5 that the relation between the total number of fibres (N_f) and number of effective (N_f^{eff}) is linear. It is worthy to note that for the series reinforced with 3DH fibres, not all fibres can be considered effective in bridging cracking, as in the case of higher fibre content, the fibres are more likely to interact with each other and there is a risk of multiple fibres pulled out together.

To quantify the overall effect of various parameters on the alignment of fibres, the orientation factor was determined according to Eq. (4). It can be seen that the series reinforced with long fibres (60 mm) had somewhat higher orientation factor than short fibres (35 mm), for both fibre content and range from 0.610 to 0.776 (see Table 6). The reason for this is that the short fibres more likely rotate through the flow of fresh materials and result in lower alignment in the direction of flow. As it can be seen from Table 6 no clear relationship between orientation factor and fibre content can be found. However, the scatter of the orientation factor values was rather low. Once again this could be related to constant casting procedure. Therefore, it can be inferred that through the casting in flow method, the orientation of long fibres could be controlled at a very satisfactory level in laboratory conditions.

3.6 Correlation of the Length Of Pull-Out Fibres and Post Cracking Behaviour

To further understand the post cracking behaviour of the hooked-end steel fibres, visible lengths of fibres on both fracture surfaces were examined. The number of fibres that are visible on both fracture surfaces according to their visible length has been categorized in intervals of 10 mm (e.g. from 0 to 10 mm, 10 to 20 mm, etc.). It can be seen that for short fibres (35 mm), the 63 % visible fibres exposed in a range of between 18 and 24 mm, while for all long fibre types (e.g. 60 mm), about 50 % have visible lengths of 30–40 mm (Fig. 6). One might say a longer visible length means the fibre pulled out through a longer distance, which should result in more energy consumption. It must be noted that for both type of 3DH steel fibres, these deformed fibres were denoted as 'fully effective fibres' (i.e. fully effective in crack bridging). While in the case of fibres hook partially deformed, they were denoted as 'partially effective fibres'. There are some non-deformed fibres found at both surfaces, which were denoted as 'non effective fibres' (see Fig. 7).

For 4DH and 5DH fibres, there are several interesting facts found from this study: (1) the full deformation of fibre hooks did not occur and only partially straightened hooks were observed; (2) these partial deformation increases with increasing fibre visible lengths; (3) although about 50 % long fibres had visible length more than half of their actual length (visible length >60/2 = 30 mm), some fibres did not deform. This is due to the fact that the mechanical deformation of the hook is not governed only by the embedded length but also by the bond strength between fibre and matrix. When the embedded length is less than the end-hook of fibres (i.e. embedded length <10 mm), the plastic deformation of the hook will not happen (see Fig. 8). Generally, if the cracking path passes close to the middle of the embedded length of a fibre, the probability of fibre deformation becomes higher; (4) as a result of unique shape and ultimate tensile strength of 5DH fibres, the high resistance to fibre pullout and multiple cracking behaviour have occurred. This could be ascribed to comparatively lower strength matrix and higher mechanical anchorage of end hook fibre. Therefore, in practice it would be more beneficial to use these types of fibres with high or ultra-high performance

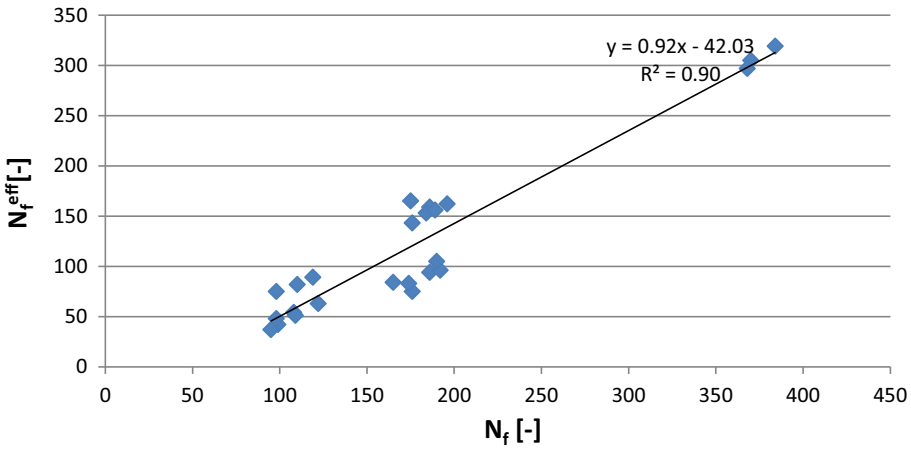

Fig. 5 Relationship between the total number of fibres and number of effective fibres at the cracked surface.

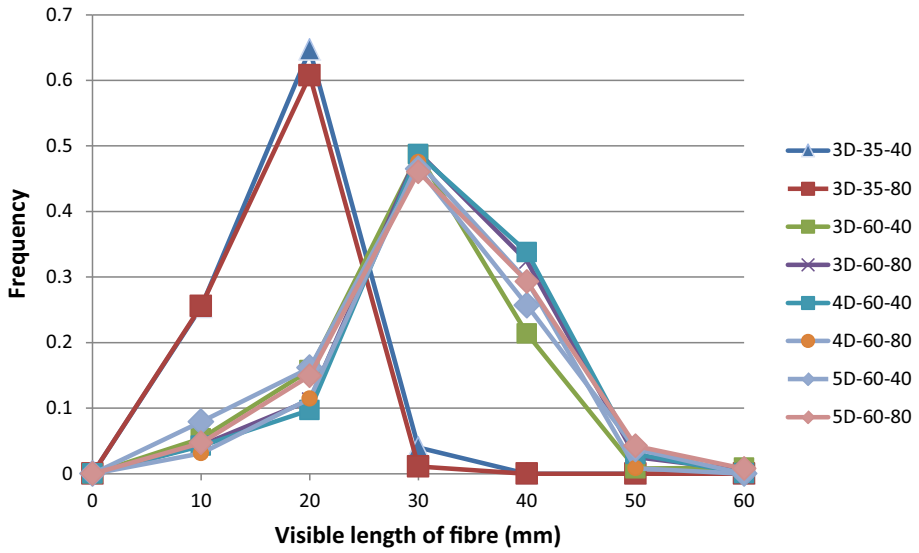

Fig. 6 Frequency of visible length of fibres which appear on fracture surface.

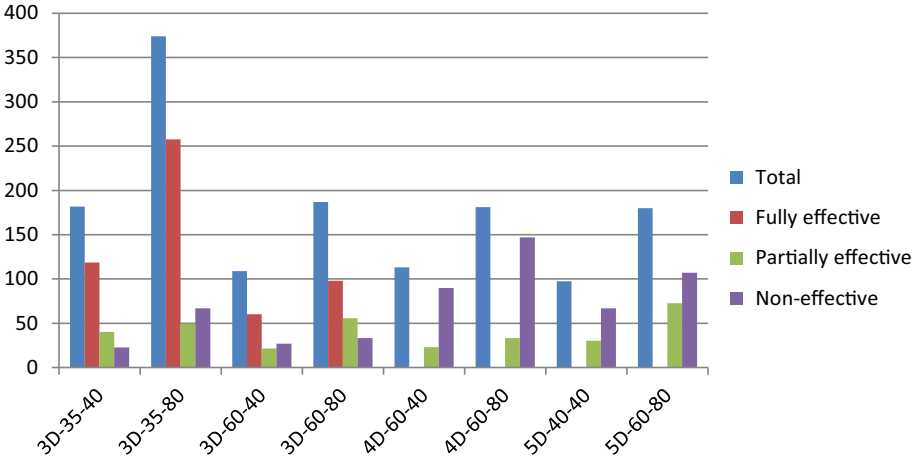

Fig. 7 The comparison between the total number of fibres and number of effective fibres on fracture surface.

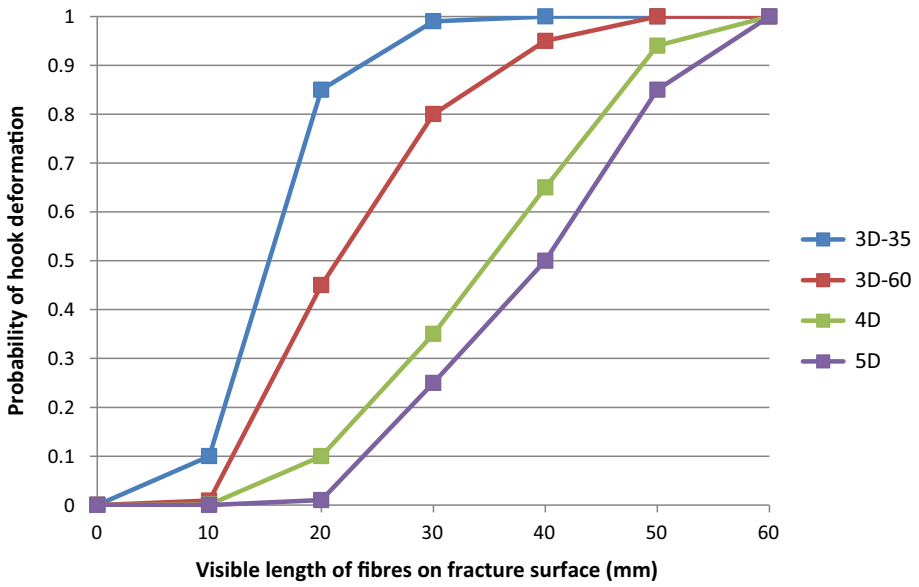

Fig. 8 Probability of fibre's hook plastic deformation with different visible length of fibres on fracture surface.

matrix, in order to assure a better mobilization and straightening of the hook during fibre pull out process. On the other hand, all series reinforced with 3DH steel fibres had only single crack initiated at the tip of the notch. In fact, most of these fibres were fully pulled out and straightened and resulted in relatively lower resistance to cracking extension.

4. Conclusions

The behaviour of various hooked-end steel fibre reinforced concretes has been fully investigated. Some major findings may be summarised as follows:

1. An addition of steel fibres up to 80 kg/m^3 had only a slightly effect on workability and compressive strength of SFRC.
2. The peak loads and residual strength of SFRC beams under 3-point bending increased with the increase of fibre dosage. The order of performance in terms of peak load was: 5DH- > 4DH- > 3DH-60- > 3DH-35. The residual loads evaluated at 4 mm CMOD was about 91, 87, 79 and 53 % of their peak load for series reinforced with 80 kg/m^3, of 5DH, 4DH, 3DH-60 and 3DH-35 respectively.
3. The residual strength was not solely related to the number of fibres counted on fracture surface, but also to the geometry of hooked-end and orientation in matrix.
4. Very good distribution and orientation of fibres in the direction of main tensile stress were obtained. The long fibre reinforced concrete had the highest values of orientation factor, indicating most likely rotation of short fibres in the perpendicular direction.
5. The fracture energy increased with the increase of fibre content and was remarkably influenced by the shape of hooked-ends. The multiple cracking and higher ductile behaviour was observed with series 5DH-80 which did not occur with other series.
6. A good balance (compatibility) between the performance of the fibres, which is highly enhanced by the shape of the hook, and the strength of the matrix shall be sought in order to optimise the capacity of both fibres and matrix in the reinforced concrete.

Open Access

References

Abrishambaf, A., Barros, J. A. O., & Cunha, V. M. C. F. (2013). Relation between fibre distribution and post-cracking behaviour in steel fibre reinforced self-compacting concrete panels. *Cement and Concrete Research, 51*, 57–66.

Astm, C. (1994). 1018, Standard test method for flexural toughness and first crack strength of fibre reinforced concrete (Using beam with third-point loading). American Society of Testing and Materials, Philadelphia, PA, Annual Book of Standard, 4. 02, pp. 509–516.

Banthia, N., & Trottier, J. (1991). Deformed steel fiber—cementitious matrix bond under impact. *Cement and Concrete Research, 21*(1), 158–168.

Bencardino, F. (2013). Mechanical parameters and post-cracking behaviour of HPFRC according to three-point and four-point bending test. *Advances in Civil Engineering*.

Beygi, M. H. A., Kazemi, M. T., Nikbin, I. M., & Amiri, J. V. (2013). The effect of water to cement ratio on fracture parameters and brittleness of self-compacting concrete. *Materials and Design, 50*, 267–276.

CNR, D. 204/2006. (2006). Guidelines for the design, construction and production control of fibre reinforced concrete structures. *National Research Council of Italy*, pp. 59.

Ding, Y. (2011). Investigations into the relationship between deflection and crack mouth opening displacement of SFRC beam. *Construction and Building Materials, 25*(5), 2432–2440.

El-Mal, H. A., Sherbini, A., & Sallam, H. (2015). Mode II fracture toughness of hybrid FRCs. *International Journal of Concrete Structures and Materials, 9*(4), 475–486.

EN, B. 12350-8: 2010 Testing fresh concrete, *Self-compacting concrete. Slump-flow test.*

EN, B. (2007). 14651: 2005 A1: 2007, *Test method for metallic fibre concrete. Measuring the flexural tensile strength (limit of proportionality (LOP), residual),* pp. 1–20.

Ferrara, L., Bamonte, P., Caverzan, A., Musa, A., & Sanal, I. (2012). A comprehensive methodology to test the performance of steel fibre reinforced self-compacting concrete (SFR-SCC). *Construction and Building Materials, 37*, 406–424.

Ferrara, L., & Meda, A. (2006). Relationships between fibre distribution, workability and the mechanical properties of SFRC applied to precast roof elements. *Materials and Structures, 39*(4), 411–420.

Giaccio, G., Tobes, J. M., & Zerbino, R. (2008). Use of small beams to obtain design parameters of fibre reinforced concrete. *Cement and Concrete Composites, 30*(4), 297–306.

Gopalaratnam, V. S., & Gettu, R. (1995). On the characterization of flexural toughness in fiber reinforced concretes. *Cement and Concrete Composites, 17*(3), 239–254.

Islam, M. S., & Alam, S. (2013). Principal component and multiple regression analysis for steel fiber reinforced concrete (SFRC) beams. *International Journal of Concrete Structures and Materials, 7*(4), 303–317.

JSCE-SF4 III, P. (1984). *Method of tests for steel fiber reinforced concrete*. Japan: The Japan Society of Civil Engineers, Concrete Library of JSCE.

Kooiman, A.G. (2000). Modelling steel fibre reinforced concrete for structural design.

Laranjeira de Oliveira, F. (2010). *Design-oriented constitutive model for steel fiber reinforced concrete.* Universitat Politècnica de Catalunya, Barcelona, Spain.

Li, H., & Liu, G. (2016). Tensile properties of hybrid fiber-reinforced reactive powder concrete after exposure to elevated temperatures. *International Journal of Concrete Structures and Materials, 10*, 1–9.

Naaman, A. E. (1972). *A statistical theory of strength for fiber reinforced concrete.*

Ozyurt, N., Mason, T. O., & Shah, S. P. (2007). Correlation of fiber dispersion, rheology and mechanical performance of FRCs. *Cement & Concrete Composites, 29*(2), 70–79.

Pająk, M., & Ponikiewski, T. (2013). Flexural behavior of self-compacting concrete reinforced with different types of steel fibers. *Construction and Building Materials, 47*, 397–408.

Rilem, T. (1985). *Determination of the Fracture Energy of Mortar and Concrete by Means of Three-point Bend Tests on Notched Beams,* pp. 285–290.

RILEM, T. (2001). 162 TDF: Design of steelfibre reinforced concrete–method, Recommendations. *Material and Structures.*

Romualdi, J. P., Ramey, M., & Sanday, S. C. (1968). Prevention and control of cracking by use of short random fibers. *Special Publication, 20*, 179–204.

Şanal, İ., & Özyurt Zihnioğlu, N. (2013). To what extent does the fiber orientation affect mechanical performance? *Construction and Building Materials, 44*, 671–681.

Sorensen, C., Berge, E., & Nikolaisen, E. B. (2014). Investigation of fiber distribution in concrete batches discharged from ready-mix truck. *International Journal of Concrete Structures and Materials, 8*(4), 279–287.

Soroushian, P., & Lee, C. (1990). Distribution and orientation of fibers in steel fiber reinforced concrete. *ACI Materials Journal, 87*(5), 433–439.

Srikar, G., Anand, G., & Prakash, S. S. (2016). A study on residual compression behavior of structural fiber reinforced concrete exposed to moderate temperature using digital image correlation. *International Journal of Concrete Structures and Materials, 10*, 1–11.

Swamy, R. (1975). Fibre reinforcement of cement and concrete. *Matériaux et Construction, 8*(3), 235–254.

Tadepalli, P. R., Dhonde, H. B., Mo, Y., & Hsu, T. T. (2015). Shear strength of prestressed steel fiber concrete I-beams. *International Journal of Concrete Structures and Materials, 9*(3), 267–281.

Vandewalle, L. (2000). RILEM TC 162-TDF: Test and design methods for steel fibre reinforced concrete. *Materials and Structures, 33*(225), 3–6.

Wecharatana, M. & Shah, S. (1983). *Fracture toughness of fiber reinforced concrete.*

Zhang, X. X., Abd Elazim, A. M., Ruiz, G., & Yu, R. C. (2014). Fracture behaviour of steel fibre-reinforced concrete at a wide range of loading rates. *International Journal of Impact Engineering, 71*, 89–96.